https://doi.org/10.5194/amt-2022-175
Preprint. Discussion started: 7 June 2022

Atmospheric Measurement Techniques Discussions

CAMP: a balloon-borne platform for aerosol particle studies in the lower atmosphere

Christian Pilz[1], Sebastian Düsing[1], Birgit Wehner[1], Thomas Müller[1], Holger Siebert[1], Jens Voigtländer[1], and Michael Lonardi[2]

[1]Leibniz Institute for Tropospheric Research, Leipzig, 04318, Germany
[2]Leipzig Institute for Meteorology, University of Leipzig, 04103, Germany

Correspondence to: Christian Pilz (pilz@tropos.de)

Abstract

Airborne observations of vertical aerosol particle distributions are crucial for detailed process studies and model improvements. Tethered balloon systems represent a less expensive alternative to aircraft to capture shallow atmospheric boundary layers (ABL). This study presents the newly developed cubic aerosol measurement platform (CAMP) for balloon-borne observations of aerosol particle microphysical properties. With an edge length of 30 cm and a weight of 9 kg, the cube is an environmentally robust instrument platform intended for measurements at low temperatures, with a particular focus on applications in cloudy Arctic ABLs. The aerosol instrumentation onboard CAMP comprises two condensation particle counters with different lower detection limits, one optical particle size spectrometer, and a miniaturized absorption photometer. Comprehensive calibrations and characterizations of the instruments were performed in laboratory experiments. The first field study with a tethered balloon system took place at the TROPOS research station in Melpitz, Germany, in the winter of 2019. At ambient temperatures between -10 and 15°C, the platform was operated up to 1.5 km height on 14 flights under a clear sky and cloudy conditions. The continuous aerosol observations at the ground station served as a reference for evaluating the CAMP measurements. During two subsequent balloon flights on the late morning of 15 February, descending layers with increased concentrations of nucleation mode particles were observed above a shallow well-mixed surface layer separated by a weakening temperature inversion. A subsequent increase in nucleation mode particles on the ground after the balloon flights suggests a downward mixing of the particles. Based on the laboratory instrument characterizations and the observations during the field campaign, CAMP demonstrated the capability to provide comprehensive aerosol particle measurements in cold and cloudy ABL.

1 Introduction

The importance of atmospheric aerosol particles to the earth's climate, given by their direct and indirect effect on the earth's radiative budget, is widely known (Bond et al., 2013; Penner et al., 2004). Airborne aerosol observations provide valuable in situ information on particle properties and spatial distributions required for improvements in process understanding and model advancement, in particular for remote areas like the Arctic (Abbatt et al., 2018; Samset et al., 2014; Schacht et al., 2019; Schmale et al., 2021; Willis et al., 2018). The extensive NETCARE aircraft campaign above the Canadian Arctic, for instance, enabled the identification of vertically varying particle properties and source regions inside and outside the Arctic ABL (Willis et al., 2019). Furthermore, substantial vertical variability of long-range transported black carbon (BC) was observed, especially at higher altitudes (Schulz et al., 2019). Detailed process studies of new particle formation (NPF) at the cloud top with subsequent particle growth (Burkart et al., 2017; Leaitch et al., 2016; Willis et al., 2017) also rest upon the NETCARE aircraft observations. Still, the open question remains whether long-range transport or local sources are more relevant for particle abundance in the Arctic. More vertical particle distribution observations in the shallow and cloudy ABL are urgently needed to address this topic.

The limited observational capabilities of aircraft in the Arctic ABL due to frequently occurring low-level mixed-phase clouds highlight the need for a different approach to complement aircraft. Tethered balloon systems (TBS) demonstrated particular capabilities for inside cloud operations under light icing conditions in the Arctic (Creamean et al., 2020; Dexheimer et al.,

https://doi.org/10.5194/amt-2022-175
Preprint. Discussion started: 7 June 2022

Atmospheric Measurement Techniques Discussions

2019; Egerer et al., 2019; Ferrero et al., 2016, 2019; Mazzola et al., 2016; Moroni et al., 2015). The high vertical resolution of TBS allows for detailed vertical aerosol distribution measurements, thus, bridging ground with aircraft observations. Moreover, the temporal evolution of aerosol layers can be observed with TBS due to their ability to hover at a constant altitude (Jensen et al., 2002). A disadvantage of TBS and uncrewed airborne systems, in general, is the restricted payload that limits to lightweight instruments or custom-built devices (Bates et al., 2013; Boer et al., 2018; Creamean et al., 2018; Porter et al., 2020; Telg et al., 2017; Zinke et al., 2021).

With the weight restrictions given by the TBS, the focus is on composing a proper configuration of mobile devices to cover the most relevant microphysical properties of Arctic aerosol particles at a high accuracy. Observations of nucleation mode particles originating from NPF in a weight-reduced configuration require a setup of two condensation particle counters (CPCs) with different lower detection limits (Heintzenberg et al., 1999; Hermann and Wiedensohler, 2001). Although many portable particle counters have been developed in recent years (e.g., Testo DiSCmini, Naneos Partector, Oxility NanoTracer), there is still a lack of commercially available lightweight CPCs with low uncertainties that are internally recording time series of particle number concentration (*N*). Measurements of the Arctic aerosol particle number size distribution (PNSD) that is dominated by Aitken and Accumulation mode particles (Tunved et al., 2013) demand optical particle size spectrometers (OPSS) with low detection limits. The low BC concentrations in the Arctic ABL that are often slightly above the detection limit of conventional full-size instruments (Backman et al., 2017) are a particular challenge for mobile devices. In the context of airborne BC observations, the required low detection limits at long averaging intervals contradict desired high spatial coverage at short intervals (Pikridas et al., 2019). Finally, a customized protective housing and a heating system are obligatory for operating sensible instruments inside clouds and at low ambient temperatures.

This study addresses the need for more vertical aerosol observations in the Arctic ABL by developing an instrumented platform for balloon-borne applications. The presented cubic aerosol measurement platform (CAMP) encases four mobile devices in a temperature-controlled and environmentally robust housing. Detailed calibrations and characterizations of the instruments were performed in laboratory studies at the World Calibration Center for Aerosol Physics (WCCAP) to ensure traceability and quality assured measurements. CAMP was tested and evaluated in a first field campaign with the BELUGA TBS (Egerer et al., 2019) at the TROPOS research station in Melpitz, Germany, in the winter of 2019. A case study from the campaign highlights the observational capabilities of CAMP and establishes a relation between lower tropospheric particle layers, ABL dynamics, and a sudden increase of nucleation mode particles on the ground.

2 Platform Overview

CAMP is a lightweight and environmentally robust instrument payload designed for in situ measurements of aerosol particle microphysics with TBS under cold weather conditions (Figure 1). With a dimension of 30 x 30 x 30 cm and a total weight of 9 kg, the platform contains two CPCs, one OPSS, and an absorption photometer. Stable measurement conditions inside the cube are maintained at temperatures above 20°C by insulation and a controlled heating system (TR12-G, Telemeter Electronic GmbH). The aerosol sampling system contains a vertical funnel inlet, a subsequent silica dryer, and a flow splitter with an integrated core sampling system. The two CPCs and the OPSS run on a shared vacuum scroll pump (V05H012A, Air Squared Manufacturing Inc.) combined with customized critical orifices. The critical pressure drop across the orifices is constantly monitored to assure constant flow rates under changing ambient pressures during balloon flights. Sample air temperature (*T*) and relative humidity (RH) are monitored with two sensors (HYT-939, B+B Thermo-Technik GmbH); one is located outside the platform downstream of the inlet and the other one inside CAMP downstream of the dryer. Another sensor (BME 280, Bosch Sensortec GmbH) acquires barometric pressure, *T*, and RH. Time and position data is provided by a satellite receiver (NL-8004U, Navilock). A microcontroller (Teensy 3.6) records the CPC and sensor data at 1 Hz on an inbuilt micro SD Card. The CPC data is also transmitted via a second microcontroller (Arduino Mega) with a radio module on 868 MHz for real-time display on the ground during balloon flights. CAMP can independently operate a minimum of three hours on one shared

https://doi.org/10.5194/amt-2022-175
Preprint. Discussion started: 7 June 2022

Atmospheric Measurement Techniques Discussions

battery, depending on ambient temperatures and resulting needs for heating. Two identical CAMPs with interchangeable instrument slots were developed.

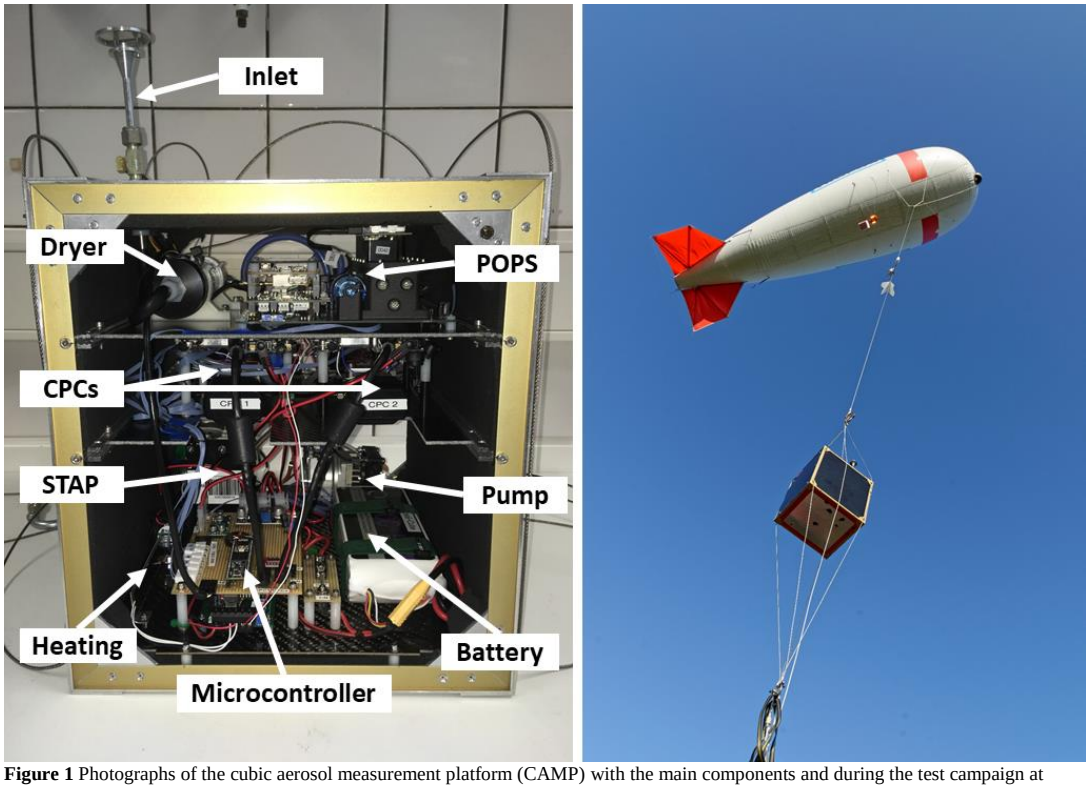

Figure 1 Photographs of the cubic aerosol measurement platform (CAMP) with the main components and during the test campaign at Melpitz with BELUGA in Winter 2019

2.1 Condensation Particle Counters

A well-characterized handheld CPC (model 3007, TSI Inc.) (Asbach et al., 2012; Hämeri et al., 2002; Mordas et al., 2008) was adapted for the instrumentation of CAMP, similarly to Altstädter et al. (2015). The weight of the CPCs was reduced from 1.5 to 0.7 kg by removing the housing, display, and batteries. An external data acquisition was established with a microcontroller over the serial interface for concentration recordings at 1 Hz. The initial flow system was substituted with an external vacuum scroll pump and a customized critical orifice to set a constant sample flow rate. The slightly different flow rate across the orifice introduced a constant offset in instrument counting efficiency that was considered with a correction factor determined by calibrations (details below). With the improvements in the flow system, the measurement uncertainties were reduced from ±20 to ±5 % for 10 s average particle number concentration relative to a calibrated reference Electrometer (3068B, TSI Inc.) for 40 nm silver particles.

Two CPCs with different lower cut-offs are commonly used on airborne platforms to detect nucleation mode particles originating from NPF by calculating the difference in concentrations between the instruments. The lower detection limit is defined as the particle diameter (D_{P50}) at which the CPC shows 50 % counting efficiency. The D_{P50} depends on the temperature difference (ΔT) between the instruments saturator and condenser (Banse et al., 2001). For the CPC 3007 on CAMP, varying ΔT were investigated with software commands to prevent hardware modifications from affecting device characteristics. Other than for full-size laboratory CPCs (Banse et al., 2001), the model 3007 does not allow for individual temperature settings for saturator and condenser because of its combined warming/cooling system with Peltier elements. Therefore, differing ΔT can only be indirectly achieved with variations of the supply voltage of the Peltier elements yet without any absolute temperature

https://doi.org/10.5194/amt-2022-175
Preprint. Discussion started: 7 June 2022

Atmospheric Measurement Techniques Discussions

information provided by the instrument. With external temperature sensors (TSIC 506, B+B Thermo-Technik GmbH) attached to the saturator and condenser, the standard and maximum voltage settings were measured to result in a ΔT of 11 K and 15.1 K, respectively. The corresponding D_{P50} at the maximum ΔT of 15.1 K was determined in calibration with silver particles at the World Calibration Center for Aerosol Physics (WCCAP) in a setup according to Wiedensohler et al. (2018). The counting efficiencies were measured against a reference Electrometer (3068B, TSI Inc.) over a five minute mean for particle diameters (D_P) ranging from 5 to 40 nm at particle number concentrations of 1000 cm^{-3}. A D_{P50} of 8 nm was found with a non-linear regression following Eq. (1):

$$Eff = Eff_{max}\left[1 - exp\left(\frac{D_{P0} - D_P}{D_{P50} - D_{P0}} \cdot ln2\right)\right] \quad (1)$$

with the maximum counting efficiency (Eff_{max}) and the particle diameter for zero counting efficiency (D_{P0}). Hämeri et al. (2002) found a D_{P50} of 10 nm for the CPC 3007 at standard settings. A difference in detection limits of one CPC at standard and one at maximum settings would be relatively small with 8 and 10 nm. Therefore, an increase in D_{P50} with lower Peltier voltage settings resulting in a lower ΔT of 9.5 K was evaluated. The results of another calibration with four modified CPCs at ΔT of 15.1 K, 11 K, and 9.5 K in the WCCAP are displayed in Figure 2, with the fitting parameters given in Table 1.

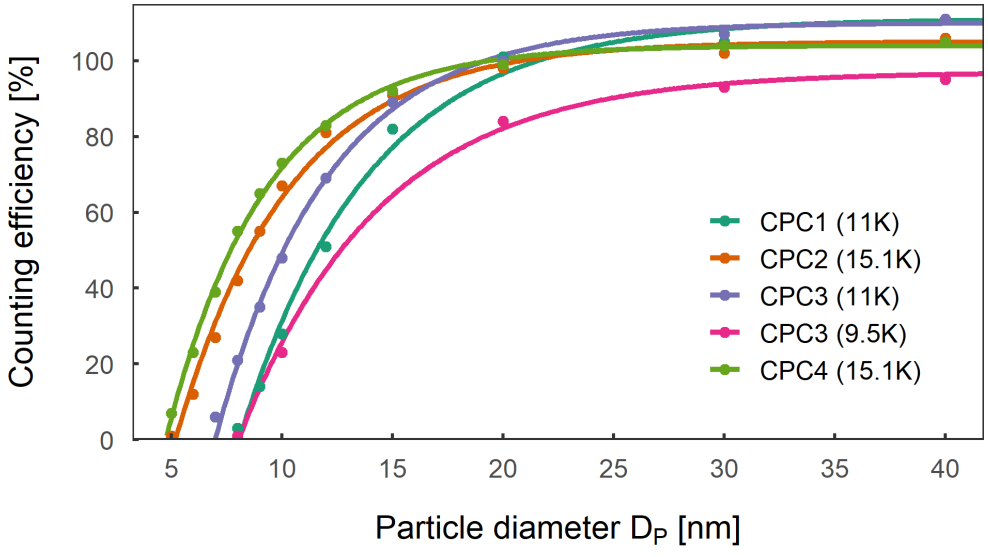

Figure 2. Regression curves of counting efficiency of four modified CPC 3007 for different Peltier voltage settings with resulting temperature differences between saturator and condenser in brackets.

CPC1 on standard settings of ΔT = 11 K showed a relatively high detection limit of 12.1 nm compared to CPC3 with 10.5 nm and former findings by Hämeri et al. (2002). A possible explanation could be slightly modified instrument characteristics caused by installing the temperature sensors for the measurements of resulting ΔT with CPC1. For CPC2 and CPC4, a D_{P50} of 7.9 nm and 8.8 nm were found at ΔT = 15.1 K. At ΔT = 9.5 K, CPC3 featured a D_{P50} of 12.4 nm with a reduced Eff_{max} compared to the calibration run with ΔT = 11 K, which probably results from a decreased degree of supersaturation. However, a ΔT of 9.5 K is suitable to achieve a more significant difference in detection limits, including the determined counting efficiency correction factor (Table 1). The final settings for CPC1 and CPC2 on CAMP1 are at ΔT of 11 K and 15.1 K resulting in lower detection limits of 12 nm (N_{12}) and 9 nm (N_9), respectively. For CPC3 and CPC4 on CAMP2, ΔT was set to 9.5 K and 15.1 K for detection limits of 12 nm (N_{12}) and 8 nm (N_8), respectively. A decrease in counting efficiency was found for the maximum setting of ΔT = 15.1 K at ambient temperature below 20°C. CAMP accounts for this temperature sensitivity by the temperature-controlled heating system.

https://doi.org/10.5194/amt-2022-175
Preprint. Discussion started: 7 June 2022

Atmospheric Measurement Techniques Discussions

Table 1 Calibration results of four CPC 3007 for different Peltier voltage settings. The correction factors account for offsets in sample flow rates from the customized flow system and reduced supersaturation in the case of CPC3 at 1.2 V. Uncertainties for the D_{P50} are derived from a non-linear regression fit.

CPC	Peltier setting [V]	ΔT [K]	D_{P50} [nm]	D_{P0} [nm]	Eff_{max} [%]	Correction factor
1	1.4	11	12.1 ± 0.4	8.1	111	0.90
2	2	15.1	8.8 ± 0.2	5.2	105	0.95
3	1.4	11	10.5 ± 0.1	7.0	110	0.91
3	1.2	9.5	12.4 ± 0.5	8.0	97	1.03
4	2	15.1	7.9 ± 0.1	4.8	104	0.96

2.2 Optical Particle Size Spectrometer

The Portable Optical Particle Spectrometer (POPS, Handix Scientific Inc.) is a lightweight instrument for PNSD measurements in an optical size range from 0.13 to 3.5 µm that was developed for application on uncrewed airborne platforms (Boer et al., 2018; Creamean et al., 2020; Gao et al., 2016; Liu et al., 2021; Telg et al., 2017). In particular, the comparably low detection limit makes the POPS suitable for measurements in the Arctic. Sizing calibrations of two POPS were performed with test particles of polystyrene latex (PSL) spheres in 14 sizes ranging from 0.125 to 3 µm. In parallel, the counting efficiencies against a reference CPC (model 3772, TSI Inc.) were analyzed for the sub-micron PSL sizes. Agglomerated PSL particles and residuals originating from the nebulizing process of PSL from a suspension were filtered out with a differential mobility analyzer (DMA) (Heim et al., 2008). The DMA was set to the mean D_P of each PSL size The calibration setup was arranged vertically to reduce losses of super-micrometer particles. On top of the setup, a nebulizer generated the test aerosol with particle-free air from a suspension. Subsequently, the particles were dehumidified by a silica dryer before entering the DMA. A flow splitter with inbuilt core sampling per line distributed the dried PSL particles to the two POPS and the reference CPC. For data evaluation, lognormal distributions were fitted to the PNSD measured by the POPS with a size resolution of 200 bins using the particle diameter bin limits provided by the manufacturer. Sizing deviations of the optical particle diameter (D_{PO}) by the POPS from the mean PSL D_P were defined by the mean mode of the lognormal fits and the sizing uncertainty from 1 standard deviation (SD) of the fit.

The results of the size calibration with PSL in Figure 3 show similar sizing deviations for the two examined POPS. Except for the PSL sizes between 0.5 and 1 µm, the sizing deviations were below 5 % for both units. In that particular particle size range, sizing deviations up to 27 % were found for both POPS. In addition, an increased sizing uncertainty of POPS1 ranging up to 23 % was seen in this size range in contrast to POPS2, showing a moderate SD of 8 %. Unit-to-unit variabilities caused POPS2 to produce a smaller SD yet with more significant sizing deviations than POPS1 with a larger SD but smaller sizing deviations. The increased variations of both POPS for PSL sizes between 0.5 and 1 µm probably result from the geometric specifications of the instrument optics that cause Mie resonances to appear in the scattering amplitude (Gao et al., 2016). Concluding from the PSL calibrations, using the POPS in configurations of 32 size channels or more is not useful as the resulting bin sizes fall below the sizing uncertainties. In addition, the errors induced by Mie resonances are avoided by using 16 bins with one single size bin covering the size range from 0.6 to 1 µm.

https://doi.org/10.5194/amt-2022-175
Preprint. Discussion started: 7 June 2022

Atmospheric Measurement Techniques Discussions

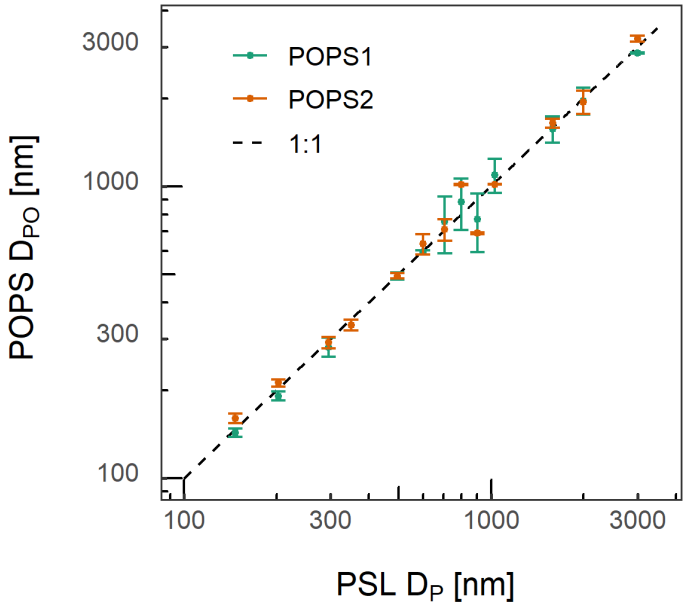

Figure 3 Measured optical particle diameter (D_{PO}) by two POPS determined by lognormal fits on the measured particle number size distribution (PNSD) of mobility diameter (D_P) selected PSL particles.

The size-resolved counting efficiency of the two POPS was evaluated starting with determining the instrument noise level with measurements of particle-free air. Integrated particle number concentrations across all size bins showed up to 10 cm^{-3} for both POPS when no particles were present at a reference CPC. The analyzed PNSD exhibited increased concentrations in bins for particles below 150 nm contributing to more than 90 % of the overall noise. A possible explanation for this is the high sensitivity of the instrument light detector to Rayleigh scattering at air molecules or stray light from apertures (Gao et al., 2016; Mei et al., 2020). In Arctic environments with low particle number concentrations, the measurement uncertainties introduced by noise in the lower bins are unacceptable. Consequently, bins below 150 nm were neglected for field measurements with the POPS on the two CAMPs. For the counting efficiency analysis, it was decided to focus on PSL sizes between 0.2 and 1 µm and evaluate the POPS particle number concentration as integral of the bins above 150 nm (N_{150}). A detailed counting efficiency analysis for Ammonium-Sulfate particles with D_P below 200 nm can be found in Mei et al. (2020). Figure 4 illustrates the counting efficiency curves of the two examined POPS determined against a reference CPC with mobility size selected PSL particles. On average, POPS1 showed a lower counting efficiency of 83 % compared to POPS2 with 109 %, thus, revealing an evident inter-unit variability. Interestingly, both units exhibit a partial decrease in efficiency for PSL sizes between 0.3 and 0.6 µm, with POPS2 showing a more pronounced reduction of 35 % from the average at D_P = 0.5 µm.

https://doi.org/10.5194/amt-2022-175
Preprint. Discussion started: 7 June 2022

Atmospheric Measurement Techniques Discussions

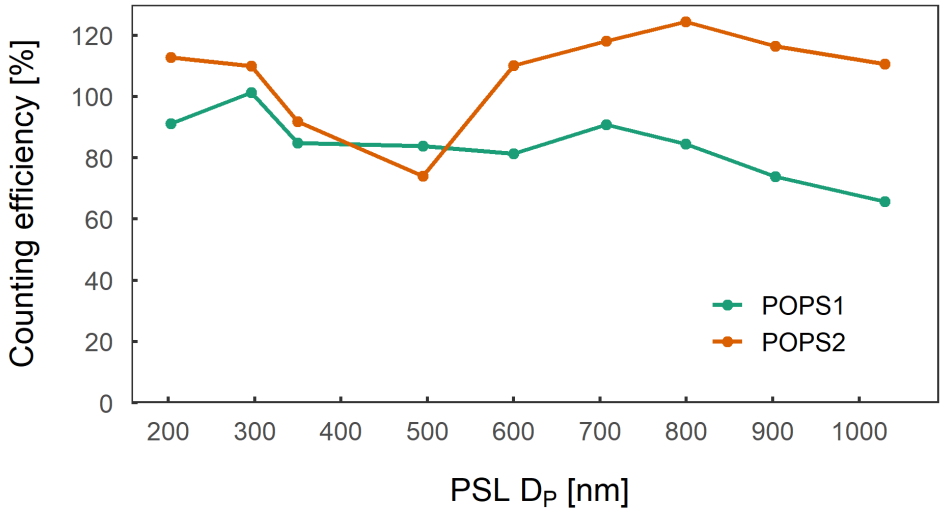

Figure 4 Counting efficiencies of two POPS measured against a reference CPC with mobility diameter (D_P) selected PSL particles.

2.3 Absorption photometer

The Single-channel Tricolor Absorption Photometer (STAP model 9406, Brechtel Manufacturing Inc.) is a filter-based instrument for the application on uncrewed airborne platforms (Bates et al., 2013; Pikridas et al., 2019; Telg et al., 2017). In principle, the STAP samples air through a filter on which aerosol particles deposit while the light intensity behind the filter (I_s) is measured at three wavelengths (λ) of 450, 525, and 624 nm. The deposited particles result in a light attenuation (ATN) that is derived in combination with a reference intensity behind a clean filter (I_r) as the logarithm of the ratio of the two light intensities denoted as the filter transmittance τ following Eq. (2):

$$\mathrm{ATN} = -\ln\left(\frac{I_s(t)}{I_r(t)} \Big/ \frac{I_s(0)}{I_r(0)}\right) = -\ln(\tau) \quad (2)$$

At the instrument initialization (t = 0 s), the ATN is reset to zero by the initial clean filter transmittance. The change in attenuation ΔATN per time step Δt is then related to the sample air column that passed through the filter during Δt yielding the light attenuation coefficient for each wavelength ($\sigma_{\mathrm{ATN}}(\lambda)$) following Eq. (3):

$$\sigma_{\mathrm{ATN}}(\lambda) = \frac{A}{Q}\frac{\mathrm{ATN}(t_2)-\mathrm{ATN}(t_1)}{t_2-t_1} = \frac{A}{Q}\frac{\Delta \mathrm{ATN}}{\Delta t}, \quad (3)$$

with the sample flow rate (Q) and the filter spot area (A). Corrections must be considered for filter loading and enhancement of $\sigma_{\mathrm{ATN}}(\lambda)$ by multiple scattering and absorption of particles deposited on the filter. An empirically determined transmittance correction term $f(\tau)$ adapted from Bond et al. (1999) and Ogren (2010) accounts for quartz fiber filter loading and enhancement following Eq. (4):

$$f(\tau) = (1.0796\,\tau + 0.71)^{-1}. \quad (4)$$

In addition, two constants, $K_1 = 0.02 \pm 0.02$ and $K_2 = 1.22 \pm 0.2$, are applied to correct for loading and enhancement by deposited scattering and absorbing particles, respectively. The particle light absorption coefficient ($\sigma_{\mathrm{abs}}(\lambda)$) from the STAP measurements is then calculated following Eq. (5):

$$\sigma_{\mathrm{abs}}(\lambda) = 0.85\frac{f(\tau)}{K_2}\frac{A}{Q}\frac{\Delta ATN}{\Delta t} - \frac{K_1}{K_2}\sigma_{\mathrm{sca}}(\lambda), \quad (5)$$

with the particle light scattering coefficient ($\sigma_{\mathrm{sca}}(\lambda)$) measured with a Nephelometer. An equivalent BC mass concentration (m_{eBC}) can be derived from $\sigma_{\mathrm{abs}}(\lambda)$ with the wavelength-dependent mass absorption cross-section (MAC(λ)) following Eq. (6):

$$m_{eBC} = \frac{\sigma_{abs}(\lambda)}{MAC(\lambda)}. \quad (6)$$

https://doi.org/10.5194/amt-2022-175
Preprint. Discussion started: 7 June 2022

Atmospheric Measurement Techniques Discussions

Two STAP units intended for the application onboard the two CAMPs were examined in the following section. Different filter materials can be used with the STAP, Pallflex filters (E70-2075W, Pall Life Sciences), and Azumi filters (371M, Azumi Filter Paper Co.). Düsing et al. (2019) reported a sensitivity of the STAP equipped with Pallflex to quick relative humidity changes by water adsorption and evaporation and provided a correction function. The Azumi filters probably show the same sensitivity due to the similar composition of glass fibers. However, the sensitivity could be less pronounced for the Azumi without the hydrophilic cellulose backing material of the Pallflex. In a comparison by Ogren et al. (2017), Azumi filters were found to increase $\sigma_{ATN}(\lambda)$ by 25 % compared to Pallflex for measurements at ambient urban aerosol with the Continuous Light Absorption Photometer (CLAP), which is the stationary version of the STAP. Since the Pallflex filters are no longer commercially available, we decided to use the Azumi filters with the STAP for this study to allow for comparison with future studies. A correction factor of 1.25^{-1} was applied for data evaluation to account for 25 % $\sigma_{ATN}(\lambda)$.

In the context of m_{eBC} measurements in the Arctic atmosphere with an absorption photometer, the lower detection limit defined by the noise level of the instrument is vital. Bates et al. (2013) determined the STAP detection limit to 0.2 Mm^{-1} at a 60 s average, which converts into m_{eBC} = 15 ng m^{-3} using an average MAC = 13.1 m^2 g^{-1} at σ_{abs}(550 nm) obtained from long-term measurements at four Arctic sites (Ohata et al., 2021). Knowledge about averaging time-dependent noise levels is crucial for airborne measurements to find an appropriate compromise between high spatial coverage resulting from short averaging times and low detection limits at extended averaging periods. Therefore, a noise analysis was performed with one STAP during the CAMP developments. The instrument noise was defined as 1 SD of $\sigma_{abs}(\lambda)$ measured during a 20-hour sampling of particle-free air on a clean Azumi filter. The internal averaging interval (Δt) was set to 1 s, and the time series of $\sigma_{abs}(\lambda)$ was calculated according to Eq. (5). The SD was evaluated for varying Δt from 1 to 180 s using arithmetic and centered moving average.

The analysis results in Figure 5 show a distinct wavelength-dependency of the STAP noise level. The centered moving average resulted in a slightly lower SD than the arithmetic average, particularly for σ_{abs}(624 nm) at Δt larger than 60 s. The STAP detection limit can be approximated by 9 Mm^{-1} $(\Delta t/s)^{-1}$ for σ_{abs}(450 nm), 14.5 Mm^{-1} $(\Delta t/s)^{-1}$ for σ_{abs}(525 nm), and 12.4 Mm^{-1} $(\Delta t/s)^{-1}$ for σ_{abs}(624 nm) when using a centered moving average. In conclusion, the averaging time must be larger than 60 s to achieve a 0.2 Mm^{-1} detection limit at all wavelengths. This requires individual data post-processing since the STAP firmware only allows for a maximum averaging time of 60 s. Occasionally varying ambient temperatures during the experiments indicated an increasing noise level with temperature. However, further investigations were unnecessary because of the controlled heating system inside CAMP. Other averaging methods that can improve temporal coverage by lower averaging times (Hagler et al., 2011) were not considered because of the capability of balloon-borne measurements to hover on constant altitudes, thus, enabling high averaging times when required.

https://doi.org/10.5194/amt-2022-175
Preprint. Discussion started: 7 June 2022

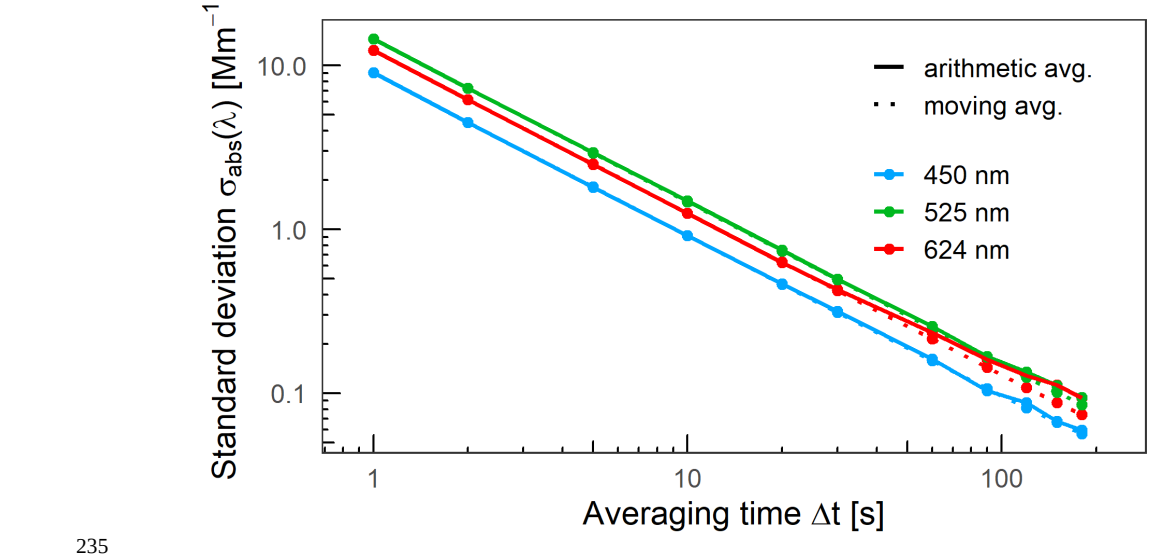

Figure 5 Standard deviation of $\sigma_{abs}(\lambda)$ in dependency of the averaging time (Δt) measured by STAP during sampling of particle-free air analyzed with arithmetic and centered moving averages.

Having defined the lower detection limit of the STAP, a laboratory evaluation of the measurement performance at low m_{eBC} was carried out. Two STAP with Azumi filters were compared against two stationary filter-based absorption photometers in a laboratory setup according to Müller et al. (2011), a Multi-Angle Absorption Photometer (MAAP 5012, Thermo Fisher Scientific Inc.) and an Aethalometer (AE33, Magee Scientific). All instruments sampled ambient urban aerosol from a mixing chamber on three consecutive days over 16 hours. The daily sampling routine started with pure ambient air progressively diluted with particle-free air up to 100% and vice versa to simulate low m_{eBC}. For data evaluation, all instruments were averaged over 120 s. The $\sigma_{abs}(\lambda)$ measurements of the STAP units were calculated using Eq. (5) with an Azumi filter correction factor of 1.25^{-1}. Because no Nephelometer data was available, $\sigma_{sca}(\lambda)$ was calculated from the ambient PNSD in the range from 10 nm to 800 nm measured by a mobility particle size spectrometer (MPSS) based on Mie-Theory. An urban aerosol refractive index of $1.51+0.01i$ was assumed (Alas et al., 2019). The disregarded scattering by particles larger than 800 nm in the Mie-calculations can introduce uncertainties in $\sigma_{sca}(\lambda)$ up to 10 %. The uncertainties in $\sigma_{sca}(\lambda)$ are not considered a significant error for the $\sigma_{abs}(\lambda)$ correction by Eq. (5). Truncation was simulated for submicron particles according to Anderson and Ogren (1998) to get the $\sigma_{sca}(\lambda)$ from the Nephelometer in Eq. (5) with an absorption Ångström exponent (AAE) derived from the AE33 at λ = 470 and 660 nm by Ångström law following Eq. (7):

$$\sigma_{\mathrm{abs}}(\lambda) = \sigma_{\mathrm{abs}}(\lambda_0)\left(\frac{\lambda}{\lambda_0}\right)^{-\mathrm{AAE}}, \quad (7)$$

To compare $\sigma_{abs}(\lambda)$ from the MAAP and AE33 measured at different wavelengths, the STAP $\sigma_{abs}(\lambda)$ were interpolated to λ = 470, 520, 637, and 660 nm with an AAE derived from the ambient mean σ_{abs}(450 nm) and σ_{abs}(624 nm) of each unit. σ_{abs}(637 nm) was calculated from m_{eBC} by MAAP with a MAC of 6.6 m^2 g^{-1} according to Müller et al. (2011) following Eq. (8):

$$\sigma_{\mathrm{abs}}(637nm) = 1.05\, m_{\mathrm{eBC}}\ \mathrm{MAC}. \quad (8)$$

For the AE33, σ_{abs} at 470, 520, and 660 nm were derived from $m_{eBC}(\lambda)$ by Eq. (6) with the λ-dependent MAC of 14.54, 13.14, and 10.35 m^2 g^{-1} (Drinovec et al., 2015), respectively, and interpolated to σ_{abs}(637 nm) by Eq. (7) from λ = 470 and 660 nm. Absorption measurements from the AE33 are systematically higher than the MAAP (Collaud Coen et al., 2010). Therefore, we derived a harmonization factor of 1.81^{-1} from a linear regression between the MAAP and the AE33 at σ_{abs}(637 nm). The factor accounts for enhanced AE33 at all wavelengths $\sigma_{abs}(\lambda)$ for comparisons with the STAP.

https://doi.org/10.5194/amt-2022-175
Preprint. Discussion started: 7 June 2022

Atmospheric Measurement Techniques Discussions

The results of the laboratory comparison in Figure 6 show an underestimation of 5% by STAP1 and a 1:1 agreement of STAP2 with the MAAP at σ_{abs}(637 nm). At σ_{abs}(470 nm) STAP1 showed 2 % and STAP2 3 % lower values; at σ_{abs}(520 nm) STAP1 showed 10 % higher values and STAP2 a 1:1 agreement, and at σ_{abs}(660 nm) STAP1 showed 8 % lower values and STAP2 a 1:1 agreement with the AE33. All linear regressions were forced through zero and featured an $R^2 \geq 0.98$. The results confirm $\sigma_{abs}(\lambda)$ enhancement of 25 % by Azumi filters with the STAP as Ogren et al. (2017) found for the CLAP and support the use of a correction factor of 1.25^{-1}.

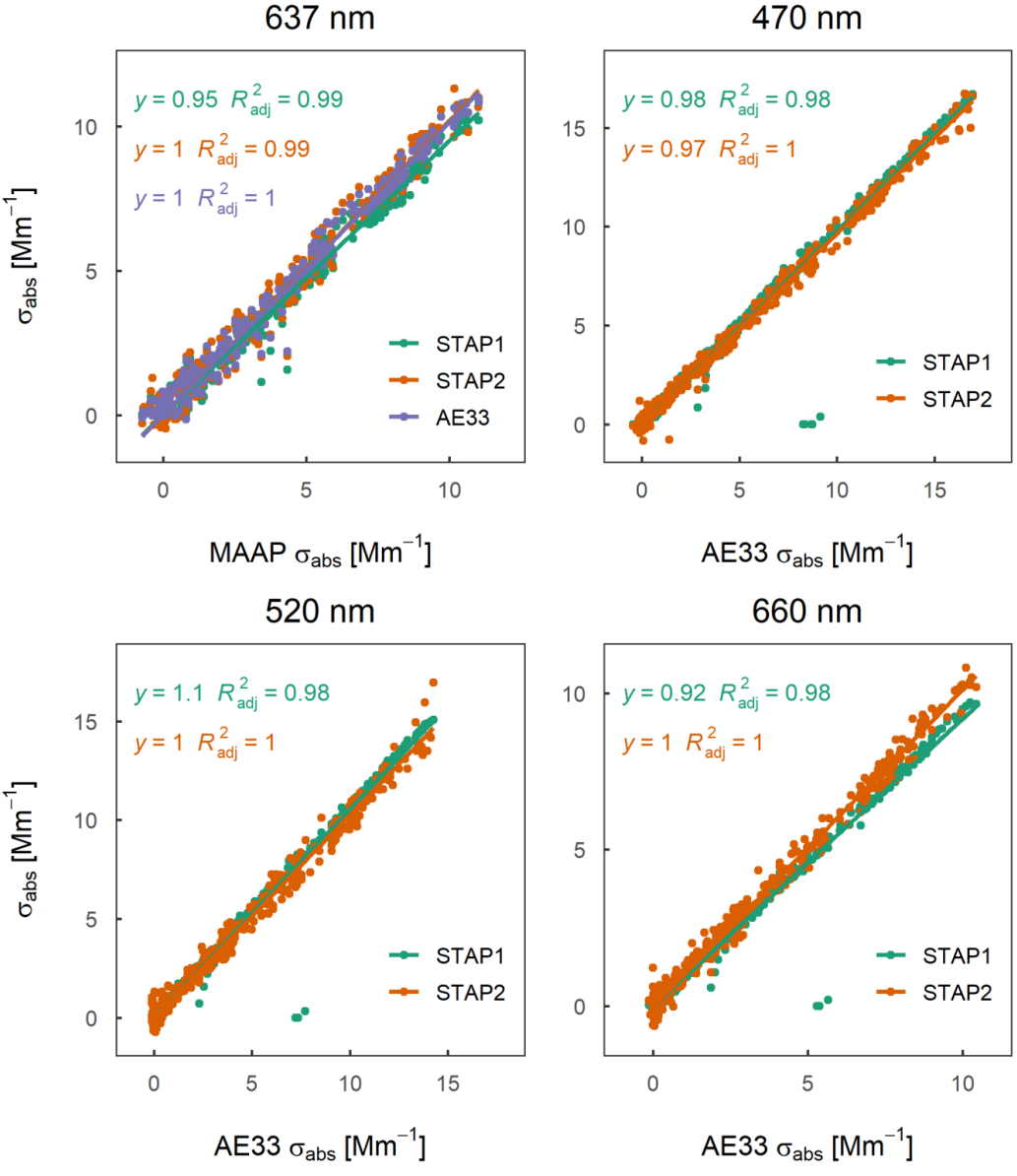

Figure 6 STAP measurements of particle light absorption coefficient $\sigma_{abs}(\lambda)$ of ambient urban aerosol variably diluted with particle-free air compared with MAAP and AE33.

https://doi.org/10.5194/amt-2022-175
Preprint. Discussion started: 7 June 2022

Atmospheric Measurement Techniques Discussions

3 First field application of CAMP

3.1 Measurement site and experiment

The first feasibility study with CAMP in the field was performed together with the BELUGA TBS at the TROPOS research station in Melpitz, Germany, in January and February 2019. CAMP was attached around 30 m below the balloon in combination with another sensor package 10 m above to measure standard meteorological parameters (T, p, RH). During profiling, the climb rates were typically below 2 m s^{-1}. Observations were made inside and outside of clouds up to maximum altitudes of 1.5 km. On five days of operation, 14 test flights were performed with CAMP in varying instrument configurations, with the data radio transmission not being operational yet. The complete instrument setup comprising CPC1 and CPC2, POPS1 in 16-bin configuration, and STAP2 was operated for two days with two flights each. The particle number concentrations in the size range from 9 to 12 nm ($N_{9\text{-}12}$) and from 12 to 150 nm ($N_{12\text{-}150}$) were derived by the difference between the two CPCs, and CPC1 and the POPS, respectively.

Ground-based long-term measurements at the Melpitz site covered meteorological parameters, the PNSD by an MPSS (TROPOS built) for mobility particle diameters from 5 to 800 nm, the PNSD by an aerodynamic particle sizer (APS 3321, TSI Inc.) for diameters from 0.5 to 10 µm, and m_{eBC} by a MAAP. A performance evaluation of CAMP measurements against the station and a detailed case study on 15 February is presented in the following sections.

3.2 CAMP performance evaluation

During varying weather conditions with ambient temperatures on the ground ranging from -10 to 15°C, the temperatures inside CAMP varied between 20°C and 30°C. Due to the silica dryer and the higher temperatures inside CAMP, the sample air RH always remained below 20 %. However, the absorption measurements of the STAP slightly increased or decreased at ambient air rapid RH changes while no variations in particle number concentrations were detected at the same altitudes (see sec. 3.3). The CAMP field measurements on ground were evaluated against the continuous observations from the Melpitz station on 15 February. N_{12}, N_9, and N_{150} of CPC1, CPC2, and the POPS1 were compared with the integrated PNSD from MPSS for the respective size ranges over 20 min scanning times. σ_{abs}(624 nm) by STAP was referenced to σ_{abs}(637 nm) by MAAP at 1 min averaging times. An average of 25 % inlet system sampling losses were seen across the four CAMP instruments compared to the stationary measurements. Consequently, a loss correction factor of 0.75^{-1} was applied to all measurements. Including the loss correction, the CPC and POPS particle number concentrations were within a 10 % uncertainty range of the MPSS. The STAP σ_{abs}(624 nm) were on average 5 % higher than the MAAP σ_{abs}(637 nm) and featured uncertainties up to 40 % for 1 min data.

A comparison of the optical PNSD detected by the POPS with the PNSD by MPSS and APS over a 20 min scanning interval is shown in Figure 7. The POPS was corrected for sampling losses and counting efficiency (see sec. 2.2), and the highest and lowest size bins were neglected because of inaccuracy. The aerodynamic particle diameter from APS was converted into mobility diameter concerning a shape factor of 1.1 (DeCarlo et al., 2004) and a particle density of 1.6 g cm^{-3} (Poulain et al., 2014). The PNSD by POPS based on PSL shows a significant underestimation of particles with diameters above 0.22 µm compared to MPSS and APS. To some extent, the underestimation by the POPS possibly comes from the partial counting efficiency decrease of the instrument, which was determined in the laboratory calibration (see chapter 2.2).

Another reason for the underestimation by POPS are differing optical properties of PSL and ambient aerosol particles. Primarily, the complex refractive index ($\tilde{n}$) determines the optical properties of ambient aerosol when assuming a spherical shape of sub-micrometer particles (Alas et al., 2019). To correct the PNSD by POPS, the theoretical response of the POPS to ambient $\tilde{n}$ was simulated based on Mie-theory with the geometric bin sizes provided by the manufacturer and the instrument optics specifications (Gao et al., 2016). A value of 1.5 was assumed for the real part of $\tilde{n}$, and for the imaginary part, values were varied between 0 and 0.02i for best fit with MPSS and APS, similar to Zieger et al. (2014).

https://doi.org/10.5194/amt-2022-175
Preprint. Discussion started: 7 June 2022

Atmospheric Measurement Techniques Discussions

The corrected PNSD by POPS with $\tilde{n}$=1.5±0.02i in Figure 7 showed the best qualitative agreement with the other instruments for sub-micrometer particles. For larger particles, the correction resulted in an artificial overestimation of particle sizes and concentrations compared to the APS. However, the $\tilde{n}$-correction intends to highlight possibilities to match the optical PNSD of the POPS with the MPSS, for instance, to derive particle mass or volume. The simulated $\tilde{n}$ for best fit might not represent the actual ambient aerosol particle properties. A different $\tilde{n}$ would be required to represent better the optical properties of super-micrometer particles (Alas et al., 2019). In addition, non-spherical and irregularly shaped particles have to be considered when comparing coarse mode PNSD from an OPSS with an APS.

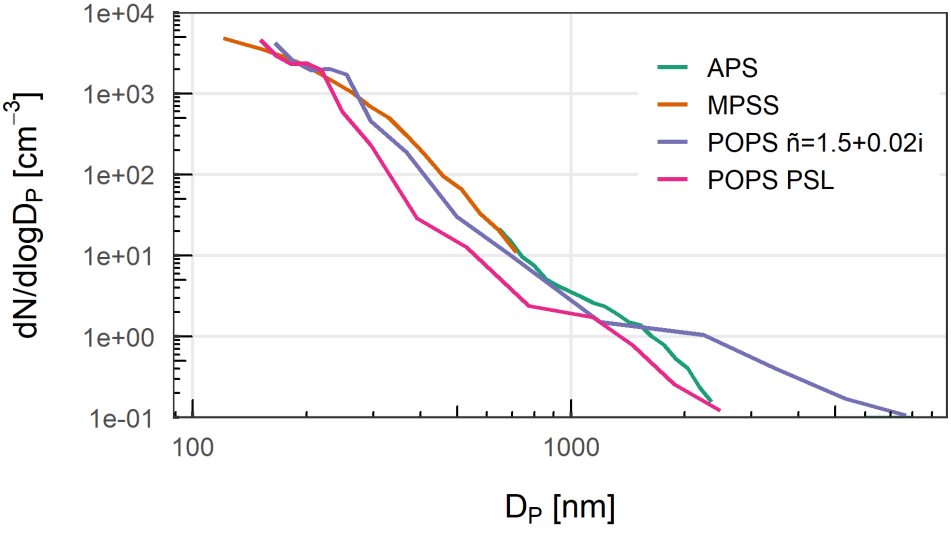

Figure 7 Mean particle number size distribution (PNSD) of POPS on the ground compared with MPSS and APS over a 20 min scanning period in Melpitz on 15 February 2019. The PSL calibrated optical PNSD from the POPS was corrected for best fit with an assumed aerosol refractive index of $\tilde{n}$=1.5+0.02i.

3.3 Case study 15 February 2019

Two balloon flights (i.e. four profiles) were performed in the late morning hours on a cloud-free day from 9:20 to 10:30 UTC and from 10:40 to 11:45 UTC. The ground-based meteorological observations in Figure 8 show a steadily increasing global radiation (G) up to 470 W m^{-2} and T from -2 up to 13°C while RH decreased from 96 to 50 % under low westerly winds ranging from 0.3 to 3.6 m s^{-1}.

https://doi.org/10.5194/amt-2022-175
Preprint. Discussion started: 7 June 2022

Atmospheric Measurement Techniques Discussions

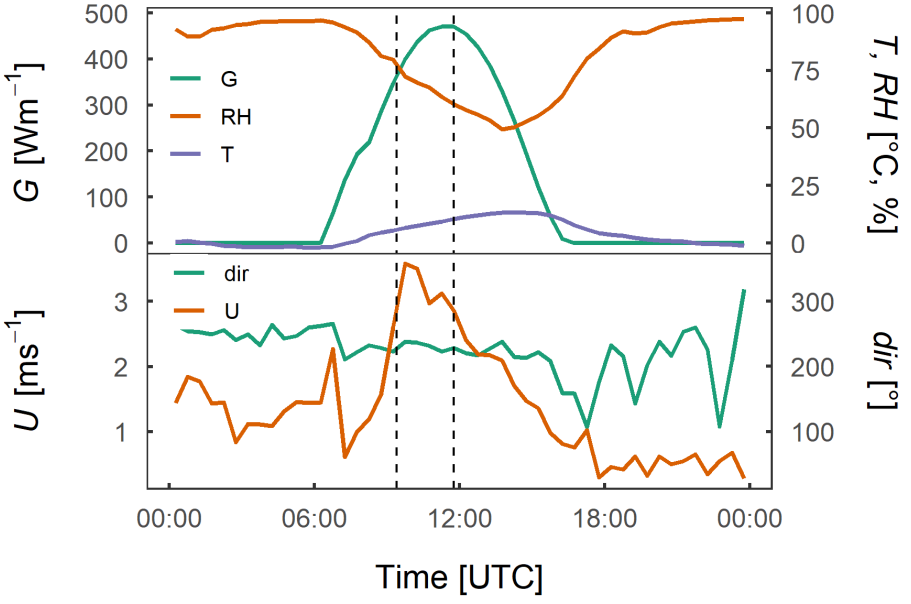

330 **Figure 8** Time series of global radiation (*G*), temperature (*T*), relative humidity (RH), wind speed (*U*), and wind direction (*dir*) at Melpitz on 15 February 2019. The vertical dashed lines mark the starting time of the first and the end of the second balloon flight.

The observed vertical profiles of potential temperature (θ) and water vapor mixing ratio (q) derived from the balloon-borne meteorological sensor package are shown in Figure 9. The θ profiles depict an almost neutrally stratified ground layer of 150 to 200 m. The well-mixed ground layer slowly warmed up through convective heating. A temperature inversion on top of the
335 mixed-layer gradually weakened from 0.02 to 0.01 K m^{-1} while lifting. Above the inversion, a stably stratified layer up to 600 m showed a gradual shift towards neutral stratification with increased humidity fluctuations higher up.

https://doi.org/10.5194/amt-2022-175
Preprint. Discussion started: 7 June 2022

Atmospheric Measurement Techniques Discussions

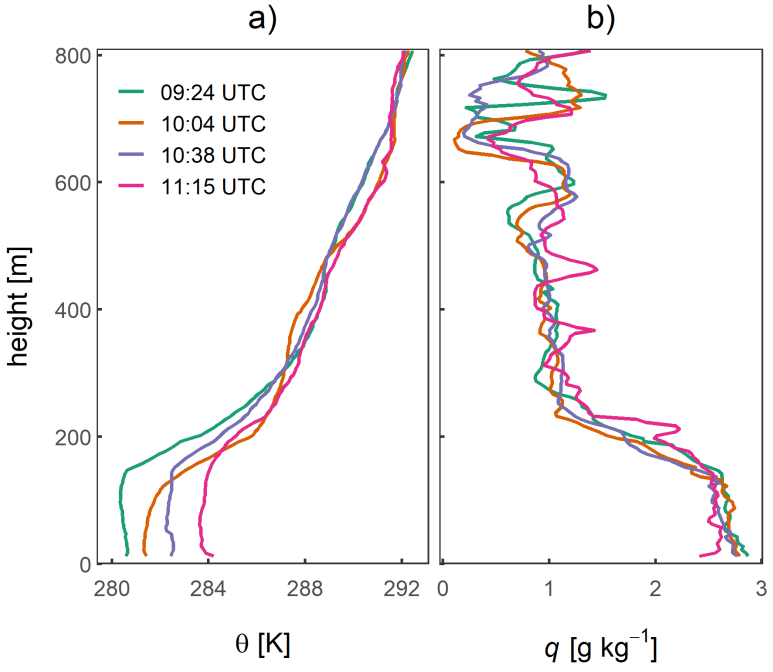

Figure 9 Vertical profiles of a) potential temperature (θ) and b) water vapor mixing ratio (q) displayed as 5 m averages. Balloon-borne observations were made during two flights in Melpitz on 15 February 2019, and displayed times represent the start of either an ascent or descent profile.

The time series of integrated aerosol PNSD at the ground in Figure 10 showed decreasing trends in $N_{12\text{-}150}$ and N_{150} with minor variability between 9:00 and 12:00 UTC. $N_{9\text{-}12}$ appeared more variable with intermittent short-term rises in the meantime. In the afternoon, a distinct increase of $N_{9\text{-}12}$ occurred over three hours leading to doubling concentrations while $N_{12\text{-}150}$ and N_{150} continued to decrease further. The mean PNSD from 12:00 and 15:00 UTC showed a nucleation mode that is not present between 9:00 and 12:00 UTC (Figure 11). The PNSD time series does not indicate NPF at the ground as the source for the suddenly occurring nucleation mode particles.

https://doi.org/10.5194/amt-2022-175
Preprint. Discussion started: 7 June 2022

Atmospheric Measurement Techniques Discussions

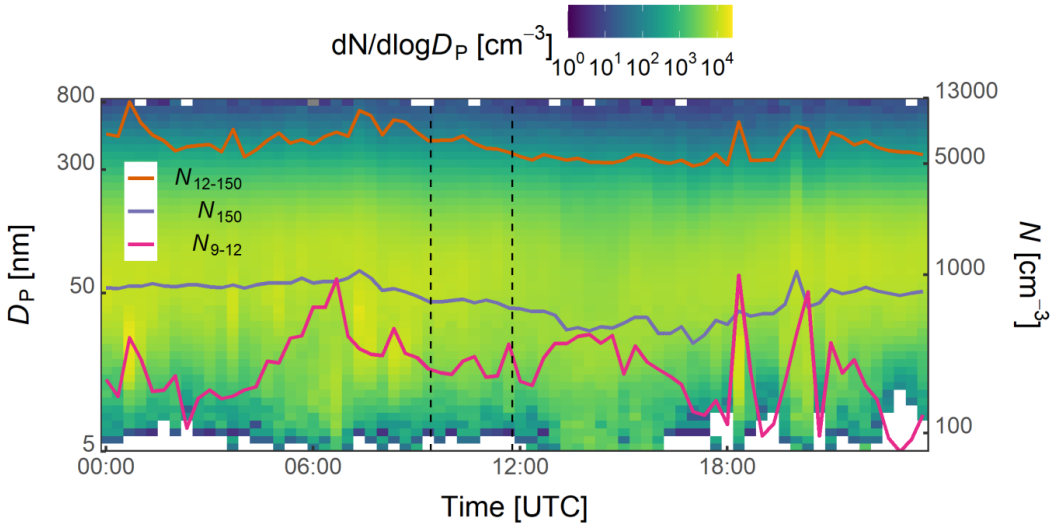

Figure 10 Time series of the PNSD and integrated particle number concentrations in size range from 9 to 12 nm ($N_{9\text{-}12}$), 12 to 150 nm ($N_{12\text{-}150}$), and above 150 nm (N_{150}) measured by MPSS at Melpitz on 15 February 2019. The vertical dashed lines mark the starting time of the first and the end of the second balloon flight.

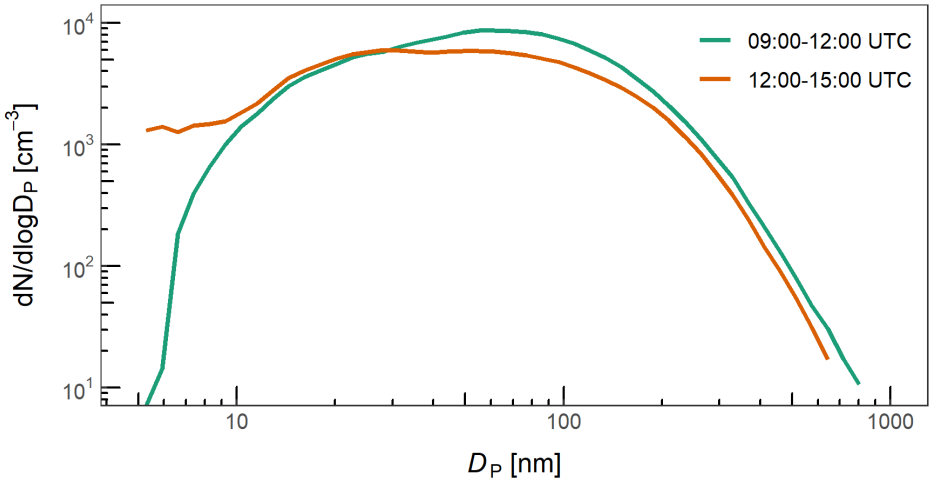

Figure 11 Mean PNSD in the late morning and early afternoon hours from MPSS measurements at Melpitz on 15 February 2019.

Balloon-borne aerosol measurements by CAMP showed different particle distributions inside the well-mixed ground layer and the stable layer above on the two balloon flights (Figure 12 and Figure 13). Inside the stably stratified layer, particle layers between 300 and 450 m showed 5 times higher $N_{9\text{-}12}$ than the ground layer. Peak $N_{9\text{-}12}$ increased from 1000 to 3500 cm^{-3} from the first to the third profile. In the meantime, the height of the layers with peak $N_{9\text{-}12}$ decreased from 430 to 310 m. Another shallow layer of increased $N_{9\text{-}12}$ was observed inside the temperature inversion on the second profile.

https://doi.org/10.5194/amt-2022-175
Preprint. Discussion started: 7 June 2022

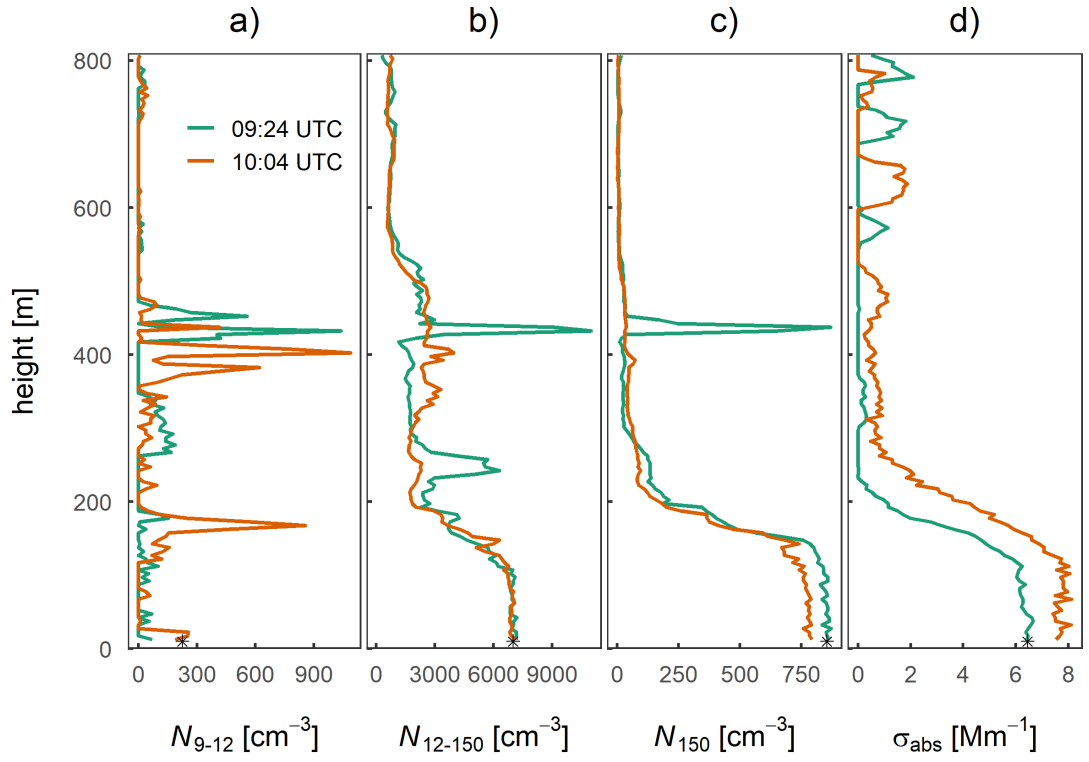

Figure 12 Vertical profiles of particle number concentrations in size range from a) 9 to 12 nm ($N_{9\text{-}12}$), b) 12 to 150 nm ($N_{12\text{-}150}$), c) 0.15 to 2.9 µm (N_{150}), and d) of the particle light absorption coefficient at 624 nm wavelengths (σ_{abs}) displayed as 5 m averages. A 60 s centered moving average was applied to $\sigma_{abs}(624)$ before taking a 5 m average. The asterisks represent the corresponding ground-based observations of integrated $N_{9\text{-}12}$, $N_{12\text{-}150}$, and N_{150} from MPSS in a) to c) and of $\sigma_{abs}(637\ nm)$ from MAAP in d) at the start of the first profile. The displayed times represent the start of the ascent or descent profile during the balloon first flight in Melpitz on 15 February 2019.

$N_{12\text{-}150}$ and N_{150} were almost constant in the well-mixed ground layer. Distinct negative gradients in $N_{12\text{-}150}$ and N_{150} at the top of the ground layer marked the transition to the stably stratified layer with a generally lower Aitken and accumulation mode particle abundance. The gradients in $N_{12\text{-}150}$ and N_{150} gradually decreased from -54 to -44 $cm^{-3}\ m^{-1}$ and from -7.0 to -4.4 $cm^{-3}\ m^{-1}$, respectively. Shallow layers of increased $N_{12\text{-}150}$ and N_{150} were observed inside the stable layer between 330 and 375 m on the first and between 430 to 450 m on the last profile. Peak $N_{12\text{-}150}$ and N_{150} were up to 2 times higher inside these two layers than in the ground layer.

The $\sigma_{abs}(\lambda)$ profiles reflect the general trend of the $N_{12\text{-}150}$ distributions with less vertical resolution due to the applied 60 s moving average. In the well-mixed ground layer, $\sigma_{abs}(\lambda)$ were relatively constant except for profile three, featuring a decreasing trend with a local minimum at 150 m height. The second $\sigma_{abs}(\lambda)$ profile seemed biased by a measurement offset inside the ground layer since ground observations agreed well with the first profile, and no distinct increase in $N_{12\text{-}150}$ or N_{150} was observed. In addition, the $\sigma_{abs}(\lambda)$ measurements above 550 m appeared to be influenced by ambient humidity changes as there were no detectable variations in $N_{12\text{-}150}$ or N_{150} at altitudes of $\sigma_{abs}(\lambda)$ changes.

https://doi.org/10.5194/amt-2022-175
Preprint. Discussion started: 7 June 2022

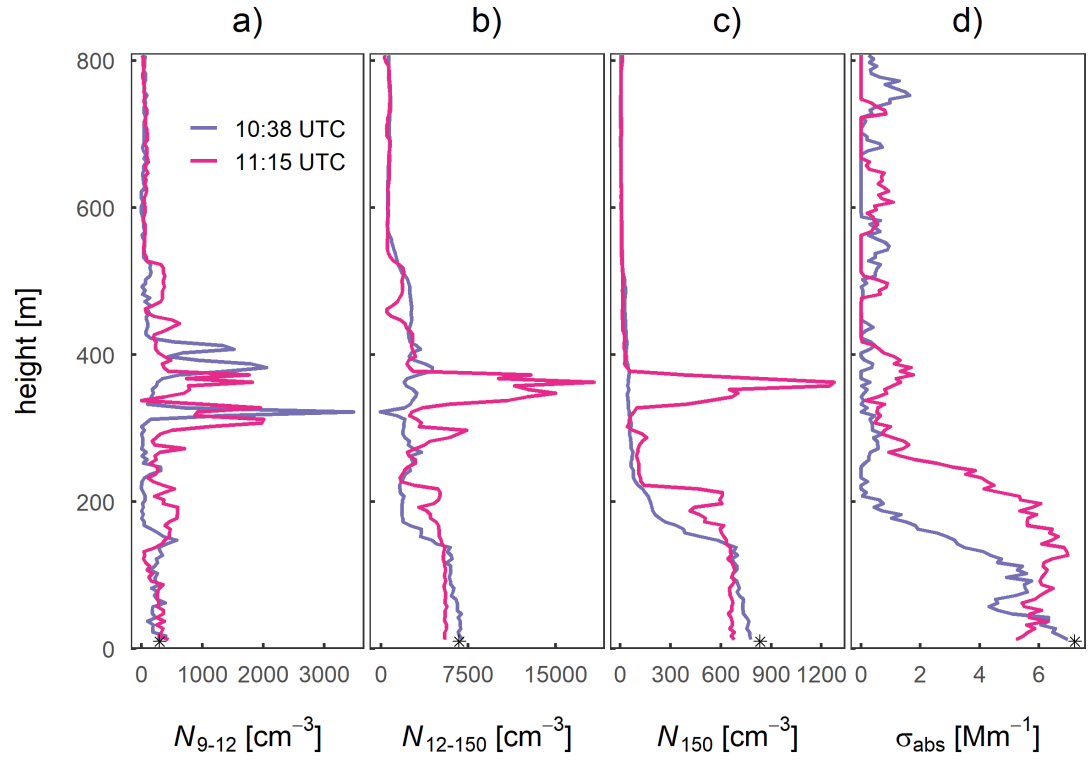

Figure 13 Same as in **Figure 12** observed during the second balloon flight in Melpitz on 15 February 2019.

From the balloon-borne and ground observations, we conclude that the layers with increased $N_{9\text{-}12}$ above the well-mixed ground layer originated from NPF and were mixed down after the balloon flight. Measured peak $N_{9\text{-}12}$ that corresponds to NPF events, the weakening temperature inversion, gradually decreasing gradients in $N_{12\text{-}150}$ and N_{150}, and the increase in $N_{9\text{-}12}$ on the ground in the afternoon support this hypothesis. The occasionally appearing plumes of increased $N_{12\text{-}150}$ and N_{150} close to the layers of increased $N_{9\text{-}12}$ did not necessarily prevent NPF in the stably stratified layer, as shown by airborne observations at a different site by Wehner et al. (2010). In particular, the appearance of increased nucleation mode particle concentrations originating from NPF on top of a well-mixed ground layer, as seen on the second profile, was previously reported from airborne observations at Melpitz in summer (Platis et al., 2016; Siebert et al., 2004). Both studies showed that turbulence and the thermodynamic conditions inside an inversion layer could create favorable conditions for NPF. Another airborne study at Melpitz by Stratmann et al. (2003) observed NPF inside a residual layer and subsequent downward mixing of nucleation mode particles after the inversion breakup. Evaluations of long-term airborne observations above Hyytiälä (Finland) by Lampilahti et al. (2021) showed that NPF is likely to occur above mixed-ground layers and emphasized the importance of downward mixing after inversion breakup. The presented case study highlights possible NPF processes at higher altitudes and their implications for particle abundance on the ground at continental sites in winter.

4 Conclusion

This study presented the newly developed CAMP for tethered balloon-borne aerosol particle observations. CAMP is designed to reliably provide observations of particle microphysical properties in cold and cloudy ABL like in the Arctic. The four instruments onboard CAMP are suitable to assess vertical distributions of Nucleation, Aitken, and Accumulation mode particle concentration, Accumulation mode PNSD, and eBC concentration. These observations enable process studies of ABL dynamics interacting with particle abundance aloft and on the ground, NPF processes at higher altitudes, and atmospheric BC

https://doi.org/10.5194/amt-2022-175
Preprint. Discussion started: 7 June 2022


Atmospheric Measurement Techniques Discussions

distribution. The set of mobile devices was calibrated and characterized in laboratory studies to provide reliable in situ measurements. Commercially available handheld CPCs were modified to achieve different lower detection limits. Nucleation mode particles originating from NPF can be identified by the difference in particle number concentrations of the two CPCS. Improvements in the CPC flow systems resulted in a significant reduction of measurement uncertainty from 20 to 5 %. Two POPS units were calibrated with size-selected PSL particles, and the results showed sizing uncertainties below 10 % when operating the instrument with 16 size bins. The mean counting efficiencies of 83 % and 109 % of the POPS were determined in the submicron particle range parallel to the calibration. For the STAP, the relation between averaging time and measurement noise was determined to enable the optimization of the temporal/spatial resolution with the required detection limit during data post-processing. A laboratory comparison of two STAP units with a MAAP and an AE33 at low eBC mass concentrations showed average deviations below 10 %.

CAMP was first tested in a field campaign with the BELUGA TBS at the TROPOS research station in Melpitz, Germany, in January and February 2019. The platform was operated on 14 balloon flights up to 1.5 km, under cloudy and clear-sky conditions, and at ambient temperatures between -10 and 15°C. Comparisons of the CAMP field measurements on the ground with MPSS from the nearby Melpitz station showed 10 % uncertainties for particle number concentrations by CPCs and POPS over 20 min averaging periods. Particle light absorption coefficients by the STAP were, on average, 5 % higher than the MAAP. The POPS optical PNSD based on PSL was compared to MPSS and APS including a refractive index correction for the POPS to find a best fit the other instruments.

A detailed case study of CAMP observations from two balloon flights and their relations to ground-based measurements on 15 February 2019 was presented. A gradually weakening temperature inversion on the cloud-free day separated the well-mixed ground layer from a stably stratified layer above. Descending layers with increased nucleation mode particle concentrations were detected inside the stable layer aloft. These layers are possibly attributed to NPF above the well-mixed ground layer. Plumes with high number concentrations of Aitken and accumulation mode particles occasionally occurred close to the nucleation mode particle layers. Half an hour after the last balloon flight, a sudden increase of nucleation mode particles occurred on the ground that suggests a downward mixing of the particles from aloft.

The results of the laboratory instrument characterizations and the first field observations demonstrate CAMP's abilities to provide reliable aerosol particle observations under challenging environmental conditions. After the first field application, the CAMP capabilities were proven during measurements with BELUGA on the international Multidisciplinary drifting Observatory for the Study of Arctic Climate (MOSAiC) expedition in the summer of 2020 (Shupe et al., 2022). CAMP enables more routine aerosol vertical distribution measurements with TBS in a wide range of locations and seasons, thus providing valuable data for particle studies and model improvements. An advantage of the small size and low weight of the platform is the possibility of collocated measurements with other instruments on larger TBS. For instance, a combination of CAMP with a sonic anemometer (Egerer et al., 2019) enables the determination of aerosol particle fluxes. Further information on particle chemistry or ice nucleating particle properties can be gained with parallel filter sampling (Creamean et al., 2018; Porter et al., 2020), or aerosol-cloud interactions can be studied with collocated cloud microphysical observations.

5 Author Contribution

CP, BW, and SD designed the CAMP platform. BW, TM, CP, and SD designed the laboratory experiments and CP and SD carried them out. HS, and BW designed and organized the BELUGA field observations and HS, BW, CP, ML, and JV carried them out. CP and SD evaluated the data from the laboratory experiments and field observations. JV designed the meteorological sensor package for the balloon observations. CP prepared the manuscript with contributions and revision from all co-authors.

https://doi.org/10.5194/amt-2022-175
Preprint. Discussion started: 7 June 2022

Atmospheric Measurement Techniques Discussions

6 Acknowledgement

We thank Kay Weinhold, Sascha Pfeiffer, and Maik Merkel for their technical support in the laboratory experiments. Special thanks go to Ralf Kaethner and the TROPOS workshops for technical and manufacturing support of CAMP. The authors thank Thomas Conrath for the technical support in the field with BELUGA during the Melpitz campaign.

7 Competing interests

The authors declare that they have no conflict of interest.

8 References

Abbatt, J. P. D., Leaitch, W. R., Aliabadi, A. A., Bertram, A. K., Blanchet, J.-P., Boivin-Rioux, A., Bozem, H., Burkart, J., Chang, R. Y. W., Charette, J., Chaubey, J. P., Christensen, R. J., Cirisan, A., Collins, D. B., Croft, B., Dionne, J., Evans, G. J., Fletcher, C. G., Ghahremaninezhad, R., Girard, E., Gong, W., Gosselin, M., Gourdal, M., Hanna, S. J., Hayashida, H., Herber, A. B., Hesaraki, S., Hoor, P., Huang, L., Hussherr, R., Irish, V. E., Keita, S. A., Kodros, J. K., Köllner, F., Kolonjari, F., Kunkel, D., Ladino, L. A., Law, K., Levasseur, M., Libois, Q., Liggio, J., Lizotte, M., Macdonald, K. M., Mahmood, R., Martin, R. V., Mason, R. H., Miller, L. A., Moravek, A., Mortenson, E., Mungall, E. L., Murphy, J. G., Namazi, M., Norman, A.-L., O'Neill, N. T., Pierce, J. R., Russell, L. M., Schneider, J., Schulz, H., Sharma, S., Si, M., Staebler, R. M., Steiner, N. S., Galí, M., Thomas, J. L., von Salzen, K., Wentzell, J. J. B., Willis, M. D., Wentworth, G. R., Xu, J.-W. and Yakobi-Hancock, J. D.: New insights into aerosol and climate in the Arctic, Atmos. Chem. Phys. Discuss., 1–60, doi:10.5194/acp-2018-995, 2018.

Alas, H. D. C., Weinhold, K., Costabile, F., Di Ianni, A., Müller, T., Pfeifer, S., Di Liberto, L., Turner, J. R. and Wiedensohler, A.: Methodology for high-quality mobile measurement with focus on black carbon and particle mass concentrations, Atmos. Meas. Tech., 12(9), 4697–4712, doi:10.5194/amt-12-4697-2019, 2019.

Altstädter, B., Platis, A., Wehner, B., Scholtz, A., Wildmann, N., Hermann, M., Käthner, R., Baars, H., Bange, J. and Lampert, A.: ALADINA - An unmanned research aircraft for observing vertical and horizontal distributions of ultrafine particles within the atmospheric boundary layer, Atmos. Meas. Tech., 8(4), 1627–1639, doi:10.5194/amt-8-1627-2015, 2015.

Anderson, T. L. and Ogren, J. A.: Determining Aerosol Radiative Properties Using the TSI 3563 Integrating Nephelometer, Aerosol Sci. Technol., 29(1), 57–69, doi:10.1080/02786829808965551, 1998.

Asbach, C., Kaminski, H., Von Barany, D., Kuhlbusch, T. A. J., Monz, C., Dziurowitz, N., Pelzer, J., Vossen, K., Berlin, K., Dietrich, S., Götz, U., Kiesling, H. J., Schierl, R. and Dahmann, D.: Comparability of portable nanoparticle exposure monitors, Ann. Occup. Hyg., 56(5), 606–621, doi:10.1093/anhyg/mes033, 2012.

Backman, J., Schmeisser, L., Virkkula, A., Ogren, J. A., Asmi, E., Starkweather, S., Sharma, S., Eleftheriadis, K., Uttal, T., Jefferson, A., Bergin, M., Makshtas, A., Tunved, P. and Fiebig, M.: On Aethalometer measurement uncertainties and an instrument correction factor for the Arctic, Atmos. Meas. Tech., 10(12), 5039–5062, doi:10.5194/amt-10-5039-2017, 2017.

Banse, D. F., Esfeld, K., Hermann, M., Sierau, B. and Wiedensohler, A.: Particle counting efficiency of the TSI CPC 3762 for different operating parameters, J. Aerosol Sci., 32(1), 157–161, doi:10.1016/S0021-8502(00)00060-4, 2001.

Bates, T. S., Quinn, P. K., Johnson, J. E., Corless, A., Brechtel, F. J., Stalin, S. E., Meinig, C. and Burkhart, J. F.: Measurements of atmospheric aerosol vertical distributions above Svalbard, Norway, using unmanned aerial systems (UAS), Atmos. Meas. Tech., 6(8), 2115–2120, doi:10.5194/amt-6-2115-2013, 2013.

Boer, G. de, Ivey, M., Schmid, B., Lawrence, D., Dexheimer, D., Mei, F., Hubbe, J., Bendure, A., Hardesty, J., Shupe, M. D., McComiskey, A., Telg, H., Schmitt, C., Matrosov, S. Y., Brooks, I., Creamean, J., Solomon, A., Turner, D. D., Williams, C., Maahn, M., Argrow, B., Palo, S., Long, C. N., Gao, R.-S. and Mather, J.: A Bird's-Eye View: Development of an Operational ARM Unmanned Aerial Capability for Atmospheric Research in Arctic Alaska, Bull. Am. Meteorol. Soc., 99(6), 1197–1212, doi:10.1175/BAMS-D-17-0156.1, 2018.

https://doi.org/10.5194/amt-2022-175
Preprint. Discussion started: 7 June 2022

Bond, T. C., Anderson, T. L. and Campbell, D.: Calibration and Intercomparison of Filter-Based Measurements of Visible Light Absorption by Aerosols, Aerosol Sci. Technol., 30(6), 582–600, doi:10.1080/027868299304435, 1999.

Bond, T. C., Doherty, S. J., Fahey, D. W., Forster, P. M., Berntsen, T., Deangelo, B. J., Flanner, M. G., Ghan, S., Kärcher, B., Koch, D., Kinne, S., Kondo, Y., Quinn, P. K., Sarofim, M. C., Schultz, M. G., Schulz, M., Venkataraman, C., Zhang, H., Zhang, S., Bellouin, N., Guttikunda, S. K., Hopke, P. K., Jacobson, M. Z., Kaiser, J. W., Klimont, Z., Lohmann, U., Schwarz, J. P., Shindell, D., Storelvmo, T., Warren, S. G. and Zender, C. S.: Bounding the role of black carbon in the climate system: A scientific assessment, J. Geophys. Res. Atmos., 118(11), 5380–5552, doi:10.1002/jgrd.50171, 2013.

Burkart, J., Willis, M. D., Bozem, H., Thomas, J. L., Law, K., Hoor, P., Aliabadi, A. A., Köllner, F., Schneider, J., Herber, A., Abbatt, J. P. D. and Richard Leaitch, W.: Summertime observations of elevated levels of ultrafine particles in the high Arctic marine boundary layer, Atmos. Chem. Phys., 17(8), 5515–5535, doi:10.5194/acp-17-5515-2017, 2017.

Collaud Coen, M., Weingartner, E., Apituley, A., Ceburnis, D., Fierz-Schmidhauser, R., Flentje, H., Henzing, J. S., Jennings, S. G., Moerman, M., Petzold, A., Schmid, O. and Baltensperger, U.: Atmospheric Measurement Techniques Minimizing light absorption measurement artifacts of the Aethalometer: evaluation of five correction algorithms, Atmos. Meas. Tech, 3, 457–474 [online] Available from: www.atmos-meas-tech.net/3/457/2010/ (Accessed 3 February 2022), 2010.

Creamean, J. M., Primm, K. M., Tolbert, M. A., Hall, E. G., Wendell, J., Jordan, A., Sheridan, P. J., Smith, J. and Schnell, R. C.: HOVERCAT: a novel aerial system for evaluation of aerosol–cloud interactions, Atmos. Meas. Tech., 11(7), 3969–3985, doi:10.5194/amt-11-3969-2018, 2018.

Creamean, J. M., Boer, G. De, Telg, H., Mei, F., Dexheimer, D., Matthew, D., Solomon, A. and Mccomiskey, A.: Assessing the vertical structure of Arctic aerosols using tethered- balloon-borne measurements, Atmos. Chem. Phys. Discuss., (October) [online] Available from: https://doi.org/10.5194/acp-2020-989, 2020.

DeCarlo, P. F., Slowik, J. G., Worsnop, D. R., Davidovits, P. and Jimenez, J. L.: Particle morphology and density characterization by combined mobility and aerodynamic diameter measurements. Part 1: Theory, Aerosol Sci. Technol., 38(12), 1185–1205, doi:10.1080/027868290903907, 2004.

Dexheimer, D., Airey, M., Roesler, E., Longbottom, C., Nicoll, K., Kneifel, S., Mei, F., Harrison, R. G., Marlton, G. and Williams, P. D.: Evaluation of ARM Tethered Balloon System instrumentation for supercooled liquid water and distributed temperature sensing in mixed-phase Arctic clouds, Atmos. Meas. Tech. Discuss., 1–30, doi:10.5194/amt-2019-117, 2019.

Drinovec, L., Močnik, G., Zotter, P., Prévôt, A. S. H., Ruckstuhl, C., Coz, E., Rupakheti, M., Sciare, J., Müller, T., Wiedensohler, A. and Hansen, A. D. A.: The "dual-spot" Aethalometer: An improved measurement of aerosol black carbon with real-time loading compensation, Atmos. Meas. Tech., 8(5), 1965–1979, doi:10.5194/amt-8-1965-2015, 2015.

Düsing, S., Wehner, B., Müller, T., Stöcker, A. and Wiedensohler, A.: The effect of rapid relative humidity changes on fast filter-based aerosol-particle light-absorption measurements: Uncertainties and correction schemes, Atmos. Meas. Tech., 12(11), 5879–5895, doi:10.5194/amt-12-5879-2019, 2019.

Egerer, U., Gottschalk, M., Siebert, H., Ehrlich, A. and Wendisch, M.: The new BELUGA setup for collocated turbulence and radiation measurements using a tethered balloon : first applications in the cloudy Arctic boundary layer, , 4019–4038, 2019.

Ferrero, L., Cappelletti, D., Busetto, M., Mazzola, M., Lupi, A., Lanconelli, C., Becagli, S., Traversi, R., Caiazzo, L., Giardi, F., Moroni, B., Crocchianti, S., Fierz, M., Mocnik, G., Sangiorgi, G., Perrone, M., Maturilli, M., Vitale, V., Udisti, R. and Bolzacchini, E.: Vertical profiles of aerosol and black carbon in the Arctic: A seasonal phenomenology along 2 years (2011-2012) of field campaigns, Atmos. Chem. Phys., 16(19), 12601–12629, doi:10.5194/acp-16-12601-2016, 2016.

Ferrero, L., Ritter, C., Cappelletti, D., Moroni, B., Močnik, G., Mazzola, M., Lupi, A., Becagli, S., Traversi, R., Cataldi, M., Neuber, R., Vitale, V. and Bolzacchini, E.: Aerosol optical properties in the Arctic: The role of aerosol chemistry and dust composition in a closure experiment between Lidar and tethered balloon vertical profiles, Sci. Total Environ., 686, 452–467, doi:10.1016/j.scitotenv.2019.05.399, 2019.

Gao, R. S., Telg, H., McLaughlin, R. J., Ciciora, S. J., Watts, L. A., Richardson, M. S., Schwarz, J. P., Perring, A. E.,

https://doi.org/10.5194/amt-2022-175
Preprint. Discussion started: 7 June 2022

Thornberry, T. D., Rollins, A. W., Markovic, M. Z., Bates, T. S., Johnson, J. E. and Fahey, D. W.: A light-weight, high-sensitivity particle spectrometer for PM2.5 aerosol measurements, Aerosol Sci. Technol., 50(1), 88–99, doi:10.1080/02786826.2015.1131809, 2016.

Hagler, G. S. W., Yelverton, T. L. B., Vedantham, R., Hansen, A. D. A. and Turner, J. R.: Post-processing method to reduce noise while preserving high time resolution in aethalometer real-time black carbon data, Aerosol Air Qual. Res., 11(5), 539–546, doi:10.4209/aaqr.2011.05.0055, 2011.

Hämeri, K., Koponen, I. K., Aalto, P. P. and Kulmala, M.: The particle detection efficiency of the TSI-3007 condensation particle counter, J. Aerosol Sci., 33(10), 1463–1469, doi:10.1016/S0021-8502(02)00090-3, 2002.

Heim, M., Mullins, B. J., Umhauer, H. and Kasper, G.: Performance evaluation of three optical particle counters with an efficient "multimodal" calibration method, J. Aerosol Sci., 39(12), 1019–1031, doi:10.1016/j.jaerosci.2008.07.006, 2008.

Heintzenberg, J., Wiedensohler, A. and Kütz, S.: Modification of a commercial condensation particle counter for boundary layer balloon-borne aerosol studies, J. Atmos. Ocean. Technol., 16(5), 597–601, doi:10.1175/1520-0426(1999)016<0597:MOACCP>2.0.CO;2, 1999.

Hermann, M. and Wiedensohler, A.: Counting efficiency of condensation particle counters at low-pressures with illustrative data from the upper troposphere, J. Aerosol Sci., 32(8), 975–991, doi:10.1016/S0021-8502(01)00037-4, 2001.

Jensen, M. L., Leck, C., Targino, A., Wehner, B., Fischer, C., Swietlicki, E. and S, A. M.: Boundary layer profiles of aerosol size distribution obtained by kites and a tethered balloon during the Arctic Ocean Expedition (AOE-2001), 15th Symp. Bound. Layers Turbul., 2–5 [online] Available from: http://gateway.webofknowledge.com/gateway/Gateway.cgi?GWVersion=2&SrcAuth=ORCID&SrcApp=OrcidOrg&DestLinkType=FullRecord&DestApp=WOS_CPL&KeyUT=WOS:000185937700045&KeyUID=WOS:000185937700045, 2002.

Lampilahti, J., Leino, K., Manninen, A., Poutanen, P., Franck, A., Peltola, M., Hietala, P., Beck, L., Dada, L., Quéléver, L., Öhrnberg, R., Zhou, Y., Ekblom, M., Vakkari, V., Zilitinkevich, S., Kerminen, V. M., Petäjä, T. and Kulmala, M.: Aerosol particle formation in the upper residual layer, Atmos. Chem. Phys., 21(10), 7901–7915, doi:10.5194/acp-21-7901-2021, 2021.

Leaitch, W. R., Korolev, A., Aliabadi, A. A., Burkart, J., Willis, M. D., Abbatt, J. P. D., Bozem, H., Hoor, P., Köllner, F., Schneider, J., Herber, A., Konrad, C. and Brauner, R.: Effects of 20-100nm particles on liquid clouds in the clean summertime Arctic, Atmos. Chem. Phys., 16(17), 11107–11124, doi:10.5194/acp-16-11107-2016, 2016.

Liu, Z., Osborne, M., Anderson, K., Shutler, J. D., Wilson, A., Langridge, J., Yim, S. H. L., Coe, H., Babu, S., Satheesh, S. K., Zuidema, P., Huang, T., Cheng, J. C. H. and Haywood, J.: Characterizing the performance of a POPS miniaturized optical particle counter when operated on a quadcopter drone, Atmos. Meas. Tech., 14(9), 6101–6118, doi:10.5194/amt-14-6101-2021, 2021.

Mazzola, M., Busetto, M., Ferrero, L., Viola, A. Pietro and Cappelletti, D.: AGAP: an atmospheric gondola for aerosol profiling, Rend. Lincei, 27(1), 105–113, doi:10.1007/s12210-016-0514-x, 2016.

Mei, F., McMeeking, G., Pekour, M., Gao, R. S., Kulkarni, G., China, S., Telg, H., Dexheimer, D., Tomlinson, J. and Schmid, B.: Performance assessment of portable optical particle spectrometer (Pops), Sensors (Switzerland), 20(21), 1–22, doi:10.3390/s20216294, 2020.

Mordas, G., Manninen, H. E., Petëjä, T., Aalto, P. P., Hämeri, K. and Kulmala, M.: On operation of the ultra-fine water-based CPC TSI 3786 and comparison with other TSI models (TSI 3776, TSI 3772, TSI 3025, TSI 3010, TSI 3007), Aerosol Sci. Technol., 42(2), 152–158, doi:10.1080/02786820701846252, 2008.

Moroni, B., Becagli, S., Bolzacchini, E., Busetto, M., Cappelletti, D., Crocchianti, S., Ferrero, L., Frosini, D., Lanconelli, C., Lupi, A., Maturilli, M., Mazzola, M., Perrone, M. G., Sangiorgi, G., Traversi, R., Udisti, R., Viola, A. and Vitale, V.: Vertical Profiles and Chemical Properties of Aerosol Particles upon Ny-Ålesund (Svalbard Islands), Adv. Meteorol., 2015, doi:10.1155/2015/292081, 2015.

Müller, T., Henzing, J. S., De Leeuw, G., Wiedensohler, A., Alastuey, A., Angelov, H., Bizjak, M., Collaud Coen, M.,

https://doi.org/10.5194/amt-2022-175
Preprint. Discussion started: 7 June 2022

565 Engström, J. E., Gruening, C., Hillamo, R., Hoffer, A., Imre, K., Ivanow, P., Jennings, G., Sun, J. Y., Kalivitis, N., Karlsson, H., Komppula, M., Laj, P., Li, S. M., Lunder, C., Marinoni, A., Martins Dos Santos, S., Moerman, M., Nowak, A., Ogren, J. A., Petzold, A., Pichon, J. M., Rodriquez, S., Sharma, S., Sheridan, P. J., Teinilä, K., Tuch, T., Viana, M., Virkkula, A., Weingartner, E., Wilhelm, R. and Wang, Y. Q.: Characterization and intercomparison of aerosol absorption photometers: Result of two intercomparison workshops, Atmos. Meas. Tech., 4(2), 245–268, doi:10.5194/amt-4-245-2011, 2011.

570 Ogren, J. A.: Comment on "calibration and intercomparison of filter-based measurements of visible light absorption by aerosols," Aerosol Sci. Technol., 44(8), 589–591, doi:10.1080/02786826.2010.482111, 2010.

Ogren, J. A., Wendell, J., Andrews, E. and Sheridan, P. J.: Continuous light absorption photometer for long-Term studies, Atmos. Meas. Tech., 10(12), 4805–4818, doi:10.5194/amt-10-4805-2017, 2017.

Ohata, S., Mori, T., Kondo, Y., Sharma, S., Hyvärinen, A., Andrews, E., Tunved, P., Asmi, E., Backman, J., Servomaa, H.,

575 Veber, D., Eleftheriadis, K., Vratolis, S., Krejci, R., Zieger, P., Koike, M., Kanaya, Y., Yoshida, A., Moteki, N., Zhao, Y., Tobo, Y., Matsushita, J. and Oshima, N.: Estimates of mass absorption cross sections of black carbon for filter-based absorption photometers in the Arctic, Atmos. Meas. Tech., 14(10), 6723–6748, doi:10.5194/amt-14-6723-2021, 2021.

Penner, J. E., Dong, X. and Chen, Y.: Observational evidence of a change in radiative forcing due to the indirect aerosol effect, Nat. 2004 4276971, 427(6971), 231–234, doi:10.1038/nature02234, 2004.

580 Pikridas, M., Bezantakos, S., Močnik, G., Keleshis, C., Brechtel, F., Stavroulas, I., Demetriades, G., Antoniou, P., Vouterakos, P., Argyrides, M., Liakakou, E., Drinovec, L., Marinou, E., Amiridis, V., Vrekoussis, M., Mihalopoulos, N. and Sciare, J.: On-flight intercomparison of three miniature aerosol absorption sensors using unmanned aerial systems (UASs), Atmos. Meas. Tech., 12(12), 6425–6447, doi:10.5194/amt-12-6425-2019, 2019.

Platis, A., Altstädter, B., Wehner, B., Wildmann, N., Lampert, A., Hermann, M., Birmili, W. and Bange, J.: An Observational

585 Case Study on the Influence of Atmospheric Boundary-Layer Dynamics on New Particle Formation, Boundary-Layer Meteorol., 158(1), 67–92, doi:10.1007/s10546-015-0084-y, 2016.

Porter, G. C. E., Sikora, S. N. F., Adams, M. P., Proske, U., Harrison, A. D., Tarn, M. D., Brooks, I. M. and Murray, B. J.: Resolving the size of ice-nucleating particles with a balloon deployable aerosol sampler: The SHARK, Atmos. Meas. Tech., 13(6), 2905–2921, doi:10.5194/amt-13-2905-2020, 2020.

590 Poulain, L., Birmili, W., Canonaco, F., Crippa, M., Wu, Z. J., Nordmann, S., Spindler, G., Prévôt, A. S. H., Wiedensohler, A. and Herrmann, H.: Chemical mass balance of 300 • C non-volatile particles at the tropospheric research site Melpitz, Germany, Atmos. Chem. Phys, 14, 10145–10162, doi:10.5194/acp-14-10145-2014, 2014.

Samset, B. H., Myhre, G., Herber, A., Kondo, Y., Li, S. M., Moteki, N., Koike, M., Oshima, N., Schwarz, J. P., Balkanski, Y., Bauer, S. E., Bellouin, N., Berntsen, T. K., Bian, H., Chin, M., Diehl, T., Easter, R. C., Ghan, S. J., Iversen, T., Kirkeväg, A.,

595 Lamarque, J. F., Lin, G., Liu, X., Penner, J. E., Schulz, M., Seland, Skeie, R. B., Stier, P., Takemura, T., Tsigaridis, K. and Zhang, K.: Modelled black carbon radiative forcing and atmospheric lifetime in AeroCom Phase II constrained by aircraft observations, Atmos. Chem. Phys., 14(22), 12465–12477, doi:10.5194/ACP-14-12465-2014, 2014.

Schacht, J., Heinold, B., Quaas, J., Backman, J., Cherian, R., Ehrlich, A., Herber, A., Huang, W. T. K., Kondo, Y., Massling, A., Sinha, P. R., Weinzierl, B., Zanatta, M. and Tegen, I.: The importance of the representation of air pollution emissions for

600 the modeled distribution and radiative effects of black carbon in the Arctic, Atmos. Chem. Phys., 19(17), 11159–11183, doi:10.5194/acp-19-11159-2019, 2019.

Schmale, J., Zieger, P. and Ekman, A. M. L.: Aerosols in current and future Arctic climate, Nat. Clim. Chang., 11(2), 95–105, doi:10.1038/s41558-020-00969-5, 2021.

Schulz, H., Zanatta, M., Bozem, H., Richard Leaitch, W., Herber, A. B., Burkart, J., Willis, M. D., Kunkel, D., Hoor, P. M.,

605 Abbatt, J. P. D. and Gerdes, R.: High Arctic aircraft measurements characterising black carbon vertical variability in spring and summer, Atmos. Chem. Phys., 19(4), 2361–2384, doi:10.5194/acp-19-2361-2019, 2019.

Shupe, M. D., Rex, M., Blomquist, B., Persson, P. O. G., Schmale, J., Uttal, T., Buck, C., Boyer, M., Hofer, J., Hamilton, J.,

Posman, K., Powers, H., Pratt, K. A., Preußer, A., Rabe, B. and Rinke, A.: Overview of the MOSAiC expedition : Atmosphere, , 1–54, 2022.

Siebert, H., Stratmann, F. and Wehner, B.: First observations of increased ultrafine particle number concentrations near the inversion of a continental planetary boundary layer and its relation to ground-based measurements, Geophys. Res. Lett., 31(9), 4–7, doi:10.1029/2003GL019086, 2004.

Stone, R. S., Herber, A., Vitale, V., Mazzola, M., Lupi, A., Schnell, R. C., Dutton, E. G., Liu, P. S. K., Li, S. M., Dethloff, K., Lampert, A., Ritter, C., Stock, M., Neuber, R. and Maturilli, M.: A three-dimensional characterization of Arctic aerosols from airborne Sun photometer observations: PAM-ARCMIP, April 2009, J. Geophys. Res. Atmos., 115(13), 1–18, doi:10.1029/2009JD013605, 2010.

Stratmann, F., Siebert, H., Spindler, G., Wehner, B., Althausen, D., Heintzenberg, J., Hellmuth, O., Rinke, R., Schmieder, U., Seidel, C., Tuch, T., Uhrner, U., Wiedensohler, A., Wandinger, U., Wendisch, M., Schell, D. and Stohl, A.: New-particle formation events in a continental boundary layer: First results from the SATURN experiment, Atmos. Chem. Phys., 3(5), 1445–1459, doi:10.5194/acp-3-1445-2003, 2003.

Telg, H., Murphy, D. M., Bates, T. S., Johnson, J. E., Quinn, P. K., Giardi, F. and Gao, R. S.: A practical set of miniaturized instruments for vertical profiling of aerosol physical properties, Aerosol Sci. Technol., 51(6), 715–723, doi:10.1080/02786826.2017.1296103, 2017.

Tunved, P., Ström, J. and Krejci, R.: Arctic aerosol life cycle: Linking aerosol size distributions observed between 2000 and 2010 with air mass transport and precipitation at Zeppelin station, Ny-Ålesund, Svalbard, Atmos. Chem. Phys., 13(7), 3643–3660, doi:10.5194/acp-13-3643-2013, 2013.

Wehner, B., Siebert, H., Ansmann, A., Ditas, F., Seifert, P., Stratmann, F., Wiedensohler, A., Apituley, A., Shaw, R. A., Manninen, H. E. and Kulmala, M.: Observations of turbulence-induced new particle formation in the residual layer, Atmos. Chem. Phys., 10(9), 4319–4330, doi:10.5194/acp-10-4319-2010, 2010.

Wiedensohler, A., Wiesner, A., Weinhold, K., Birmili, W., Hermann, M., Merkel, M., Müller, T., Pfeifer, S., Schmidt, A., Tuch, T., Velarde, F., Quincey, P., Seeger, S. and Nowak, A.: Mobility particle size spectrometers: Calibration procedures and measurement uncertainties, Aerosol Sci. Technol., 52(2), 146–164, doi:10.1080/02786826.2017.1387229, 2018.

Willis, M. D., Köllner, F., Burkart, J., Bozem, H., Thomas, J. L., Schneider, J., Aliabadi, A. A., Hoor, P. M., Schulz, H., Herber, A. B., Leaitch, W. R. and Abbatt, J. P. D.: Evidence for marine biogenic influence on summertime Arctic aerosol, Geophys. Res. Lett., 44(12), 6460–6470, doi:10.1002/2017GL073359, 2017.

Willis, M. D., Leaitch, W. R. and Abbatt, J. P. D.: Processes Controlling the Composition and Abundance of Arctic Aerosol, Rev. Geophys., 56(4), 621–671, doi:10.1029/2018RG000602, 2018.

Willis, M. D., Bozem, H., Kunkel, D., Lee, A. K. Y., Schulz, H., Burkart, J., Aliabadi, A. A., Herber, A. B., Richard Leaitch, W. and Abbatt, J. P. D.: Aircraft-based measurements of High Arctic springtime aerosol show evidence for vertically varying sources, transport and composition, Atmos. Chem. Phys., 19(1), 57–76, doi:10.5194/acp-19-57-2019, 2019.

Xu, J. W., Martin, R. V., Morrow, A., Sharma, S., Huang, L., Richard Leaitch, W., Burkart, J., Schulz, H., Zanatta, M., Willis, M. D., Henze, D. K., Lee, C. J., Herber, A. B. and Abbatt, J. P. D.: Source attribution of Arctic black carbon constrained by aircraft and surface measurements, Atmos. Chem. Phys., 17(19), 11971–11989, doi:10.5194/acp-17-11971-2017, 2017.

Zieger, P., Fierz-Schmidhauser, R., Poulain, L., Müller, T., Birmili, W., Spindler, G., Wiedensohler, A., Baltensperger, U. and Weingartner, E.: Influence of water uptake on the aerosol particle light scattering coefficients of the Central European aerosol, Tellus, Ser. B Chem. Phys. Meteorol., 66(1), doi:10.3402/tellusb.v66.22716, 2014.

Zinke, J., Salter, M. E., Leck, C., Lawler, M. J., Porter, G. C. E., Adams, M. P., Brooks, I. M., Murray, B. J. and Zieger, P.: The development of a miniaturised balloon-borne cloud water sampler and its first deployment in the high Arctic, https://doi.org/10.1080/16000889.2021.1915614, 73(1), 1–12, doi:10.1080/16000889.2021.1915614, 2021.